

Optical and structural characterisation of single and multilayer germanium/silicon monoxide systems

G. Pérez^{a,*}, A.M. Bernal-Oliva^b, E. Márquez^b, J.M. González-Leal^b, C. Morant^c,
I. Génova^a, J.F. Trigo^d, J.M. Sanz^c

^aCIDA, Arturo Soria 289, E-28033 Madrid, Spain

^bDepartamento Física de la Materia Condensada, Universidad de Cádiz, E-11510 Puerto Real, Cádiz, Spain

^cDepartamento Física Aplicada, Universidad Autónoma de Madrid, Cantoblanco, E-28049 Madrid, Spain

^dDepartamento Energías Renovables, CIEMAT, Avda. Complutense 22, E-28040 Madrid, Spain

Received 25 June 2004; received in revised form 23 January 2005; accepted 30 March 2005

Available online 23 May 2005

Abstract

Germanium and silicon monoxide thin films prepared with different evaporation conditions are analysed. Substrate temperatures from 30 to 370 °C and deposition rates from 0.3 to 3.0 nm/s for SiO and from 0.5 to 1.5 nm/s for Ge films are considered. Optical constants in the mid-infrared range are derived from transmission spectra and their variation with deposition conditions is related to structural and morphological changes in the films. Taking into account the results of the single layers study, deposition conditions adequate for both SiO and Ge thin films in multilayer optical coatings for the mid-infrared range of the spectrum are selected. The optical characterisation of a ten-layer bandpass filter, designed considering the experimental optical constants for both materials and prepared with the selected deposition conditions, is presented. The results indicate that the departure of experimental transmittance in the mid-infrared range from the design is mainly due to thickness deviations.

© 2005 Elsevier B.V. All rights reserved.

Keywords: Germanium; Silicon oxide; Optical properties; Optical coatings

1. Introduction

Multilayer optical coatings for the mid-infrared range, between 3 and 5 μm , are used in many devices, e.g. optical systems for space, gas sensors, etc [1–5]. Germanium and silicon monoxide thin films are suitable for these applications as they are both transparent in that region of the spectrum, have significantly different refractive indices [6] and are well known to be chemically and mechanically compatible in multilayer stacks [1,3,7].

Germanium is frequently used as high refractive-index material in multilayer interference coatings for the infrared range [1,3,5,7–11]. Ge thin films were analysed in detail in the 70's as representative of amorphous materials [12–17] in terms of the continuous random network model [18].

More recent papers [19–21] report the improvement of some film properties (e.g. adherence, density, absorption in the infrared range, etc) when the films are obtained by more complex and expensive ion- or laser-assisted growth processes. The most recent studies are devoted to the electrical characterisation of the films for applications in infrared laser radiation detectors [22–25], in flat panels or in solar cells [26] and to the analysis of photoluminescence properties of Ge nanocrystals for applications in optoelectronics [27,28].

Silicon monoxide is also frequently used as a low-index material in interference coatings for mid-infrared [1,3,7] and as protective coating for metallic mirrors [29]. Many papers are devoted to the study of the optical and structural properties of silicon oxides and their dependence on deposition conditions [30–37]. Most of these papers report on the examination of experimental optical constants and of the absorption band related to Si–O–Si bond stretching, in

* Corresponding author. Tel.: +34 91 395 45 40; fax: +34 91 766 16 48.

E-mail address: gperezaq@oc.mde.es (G. Pérez).

terms of the mixture [38] or the random bonding model [39,40]. Apart from the optical applications, SiO_x layers have been analysed for light-emission devices, using the visible photoluminescence observed when $x < 1$ [37] and in microelectronics, as protective and passivation layers [31].

For the reliable preparation of multilayer optical coatings, it is of primary importance to carry out a previous research on the optical, and structural properties of single layers of the materials involved. The aim of that analysis is to obtain the best deposition conditions for each material, according to the intended application [5,41–43], and to derive the experimental optical constants of the films [44–47].

The aim of this paper is to perform an optical and structural characterisation of germanium and silicon monoxide thin films and to use these results to select the deposition conditions of multilayer coatings involving both materials, as well as to analyse the multilayers' optical properties.

2. Experimental details

2.1. Sample preparation

Single germanium and silicon monoxide films with nominal thickness of 1800 nm were deposited on polished sapphire substrates by electron beam and thermal evaporation, respectively. Deposition conditions of the films are included in Table 1 for Ge samples and in Table 2 for SiO samples. Substrate temperature was varied from room temperature to 370 °C for films grown at 0.9 nm/s. In addition, some samples were deposited at different rates for a fixed substrate temperature of 200 °C. The films were thick enough to enable several interference extrema in the transmission spectrum and, therefore, to allow a reliable determination of the optical constants.

Ten-layer coatings alternating Ge and SiO were also deposited on sapphire substrates at 200 °C with a base pressure of 2×10^{-4} Pa. The deposition rate and final thickness of the layers (around 600 nm for SiO films and

Table 1
Deposition conditions and optical properties of germanium thin films

Sample	T_s (°C)	ν (nm/s)	$n_{4\mu\text{m}}$	d_{exp} (nm)	E_g (eV)	$B^{1/2}$ ($\text{eV}^{1/2}\text{cm}^{-1/2}$)
1	30	0.9	4.21	1662	0.71	445
2	140	0.9	4.23	1592	0.75	463
3	200	0.5	4.25	1689	0.82	537
4	200	0.9	4.24	1579	0.82	543
5	200	1.5	4.26	1617	0.82	551
6	300	0.9	4.20	1598	0.90	609
7	370	0.9	4.06	1595	0.77	402

T_s is the substrate temperature and ν the deposition rate. d_{exp} and $n_{4\mu\text{m}}$ are the experimental thickness and refractive index at $\lambda = 4\mu\text{m}$, respectively. E_g and $B^{1/2}$ are the parameters of the Tauc model for the absorption coefficient [17].

Table 2
Deposition conditions and optical properties of silicon monoxide thin films

Sample	T_s (°C)	ν (nm/s)	$n_{4\mu\text{m}}$	d_{exp} (nm)
1	30	0.9	1.872	1675
2	140	0.9	1.875	1652
3	200	0.3	1.854	1611
4	200	0.9	1.880	1308
5	200	3.0	1.886	1492
6	300	0.9	1.865	1854
7	370	0.9	1.876	1518

T_s is the substrate temperature and ν the deposition rate. d_{exp} and $n_{4\mu\text{m}}$ are the experimental thickness and refractive index at $\lambda = 4\mu\text{m}$, respectively.

from 250 to 500 nm for Ge films) were controlled by a quartz-crystal monitor.

2.2. Sample characterisation

Transmission spectra of germanium samples at normal incidence were measured with two different double-beam dispersive equipments (Perkin-Elmer Lambda 9 and 781), in order to cover the whole wavelength range from 0.9 to 5 μm . For the silicon monoxide films and multilayer systems, the transmittance was measured between 1.25 and 5 μm using a Fourier Transform Infrared system with a modified optical system to improve its photometric accuracy (Perkin-Elmer Spectrum GX).

Optical-constant determination for all the samples was performed by the reverse synthesis of the transmission spectra [44,48]. For the sapphire substrates, optical constants from Ref. [49] were used. The analysis in the transparent region of both Ge and SiO films was carried out in terms of the dispersion function proposed by Wemple-DiDoménico [50] for the refractive index, on the basis of the single-oscillator approach:

$$n^2(E) = 1 + \frac{E_0 E_d}{E_0^2 - E^2} \quad (1)$$

where E_0 and E_d are the oscillator and dispersion energies, respectively, and an exponential function [51] for the extinction coefficient:

$$k(\lambda) = C e^{-\frac{(\lambda-D)}{E}} \quad (2)$$

where C , D and E are constants. Germanium thin films were also studied in the region of the absorption edge, from 0.9 to 1.4 μm , considering the function proposed by Tauc [17]:

$$\alpha(E) = B \frac{(E - E_g)^2}{E} \quad (3)$$

where E_g is the optical band gap and B is a parameter related to the semiconductor structural order. The main results obtained from the optical characterisation are included in Table 1 for Ge and Table 2 for SiO films.

In addition, reflection ellipsometric measurements of Ge thin films were used to determine the optical constants in the wavelength range from 0.28 to 0.83 μm ($1.5 < h\nu < 4.5$

eV). These data were analysed in terms of the Maxwell–Garnett EMA model, including a surface layer of different characteristics.

Structural characterisation of the Ge films was performed by X-ray diffraction, using Cu K_{α} radiation ($\lambda = 1.542 \text{ \AA}$). Atomic force microscopy, AFM, was used for morphological characterisation. The AFM images were obtained in contact mode, under ambient conditions using silicon nitride cantilevers. From the topographic images, the surface roughness was estimated in terms of the root mean square (rms) of the peak-valley statistical distribution in the images. The mean size of the observed features was derived from the analysis of different line-profiles along the sample surface.

3. Results and discussion

3.1. Ge thin films

Several germanium thin films, grown at different substrate temperatures and deposition rates, have been studied. Table 1 summarises the deposition conditions and the results of their optical characterisation.

Fig. 1 shows the X-ray diffraction pattern of samples 4, 6 and 7 (cf. Table 1). Samples 4 and 6, grown at temperatures of 200 and 300 °C, show almost featureless patterns as a clear indication of the amorphous structure of these films. On the contrary, sample 7 (grown at 370 °C) shows a pattern with three sharp peaks at angles 2θ equal to 25.86°, 45.46° and 53.80°, which correspond to the Bragg planes (111), (220) and (331), respectively, as indicated in the figure. The most intense peak corresponds to the (220) planes, in agreement with the results reported by other authors [22,23] for germanium thin films grown at similar substrate temperatures.

Representative AFM images of samples 1, 4 and 6 are shown in Fig. 2. The analysis of these images shows that increasing the substrate temperature, T_s , from 30 up to 200 °C

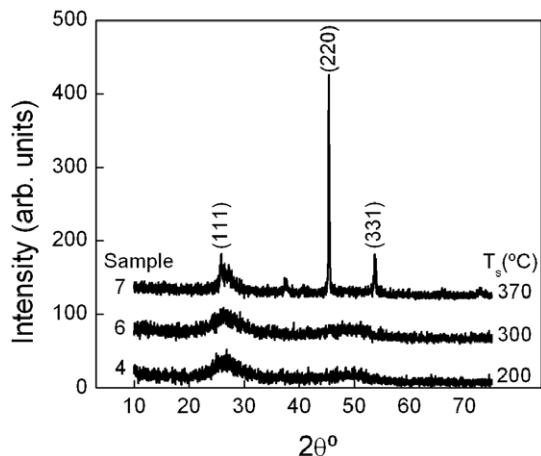


Fig. 1. XRD diffraction patterns of Ge thin films deposited on sapphire substrates at different temperatures.

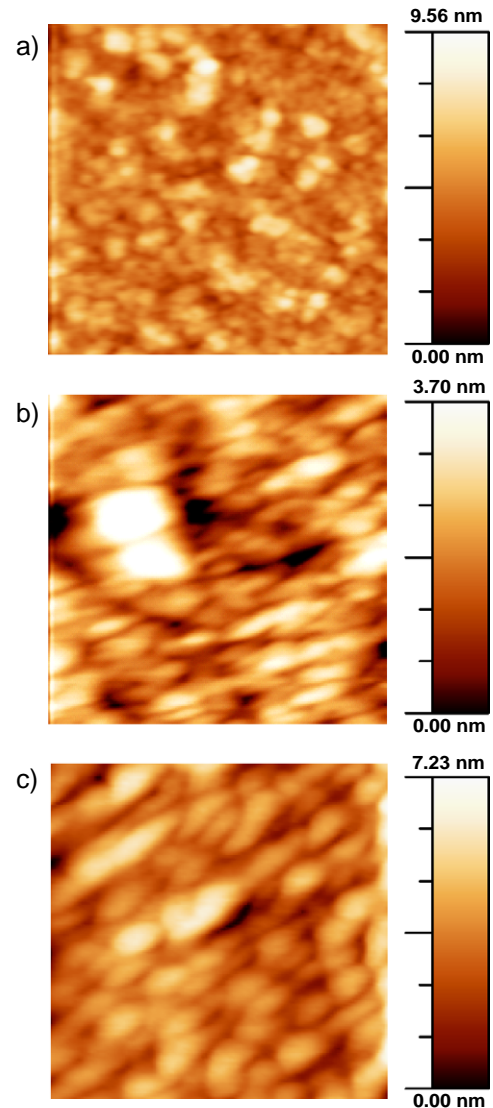


Fig. 2. AFM topographic images ($1 \times 1 \mu\text{m}^2$) of the surfaces of Ge thin films deposited on sapphire substrates at different temperatures. a) 30 °C, sample 1; b) 200 °C, sample 4; c) 300 °C, sample 6 (cf. Table 1).

results in a clear increase of the mean grain size from 60 nm for sample 1 (Fig. 2a) to 125 nm for sample 4 (Fig. 2b), while the rms roughness remains around 1.1 nm for both samples. A further increase of T_s up to 300 °C does not seem to affect the mean grain size (i.e. 115 nm), but gives rise to the formation of grooves in the film surface (cf. Fig. 2c) and a subsequent increase of the rms roughness up to 1.5 nm. It is important to note that AFM images of sample 7, grown at 370 °C, could not be obtained due to its high surface roughness.

Table 1 indicates that the refractive index of germanium thin films at $4 \mu\text{m}$ ($n_{4 \mu\text{m}}$) ranges between 4.20 and 4.26, except for the sample deposited at 370 °C (sample 7) for which $n_{4 \mu\text{m}}$ reduces to 4.06. This index value is in fact close to the value of 4.0 reported for crystalline germanium [6]. Refractive index and extinction coefficient as a function of the wavelength in the transparent region (2–5 μm) are depicted in Fig. 3. The refractive index for

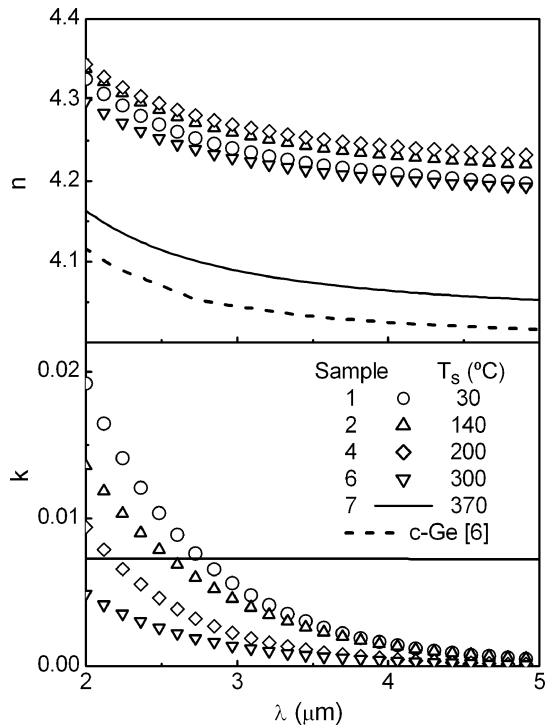


Fig. 3. Optical constants of Ge thin films deposited on sapphire substrates at different temperatures (cf. Table 1), estimated by reverse synthesis of transmission spectra.

crystalline germanium (as published by Palik [6]) is also included. The extinction coefficient is always lower than 10^{-5} for the wavelength range considered in Fig. 3. The results suggest that, whereas changes in the deposition rate have a negligible effect, at least within the range of variation studied here, the substrate temperature has a significant influence on the optical constants of the germanium films.

The analysis of transmission spectra in the region of high absorption, according to the model developed by Tauc [17], results in an optical gap (E_g) of 0.71 eV for the sample grown at room temperature (sample 1). This value of E_g is in agreement with the results reported by Connell et al. [16] for germanium films deposited by sputtering. Increasing the substrate temperature up to 300 °C leads to a more abrupt absorption edge, as indicated by the value of $B^{1/2}$ in Table 1, and to a shift of the edge to higher energies.

For wavelengths below the absorption edge, the optical constants of germanium films have been obtained from ellipsometric measurements. Fig. 4 shows the refractive index and extinction coefficient of samples prepared at different temperatures for photon energies between 1.5 and 4.5 eV ($0.28 < \lambda < 0.83 \mu\text{m}$). The values published by Palik [6] for crystalline germanium are also included. Films deposited at temperatures up to 300 °C show a smooth dependence of both optical constants with photon energy, indicating that the structure of the films is amorphous [15]. On the contrary, the behaviour of sample 7, grown at 370 °C, is similar to that of crystalline

germanium, indicating rather clearly the polycrystalline structure of the film [15].

The analysis of ellipsometric measurements of the Ge thin films, assuming the Maxwell–Garnett effective medium model and including a surface layer, confirms that the samples prepared at substrate temperatures up to 300 °C are amorphous, while sample 7 contains both crystalline and amorphous components in an approximate proportion of 80% and 20%, respectively. Furthermore, all the four samples studied by ellipsometry have a surface layer with thickness increasing from 4 to 8 nm when the substrate temperature varies from room temperature to 370 °C. This surface layer is characterised by a lower refractive index that can be caused by the presence of roughness (i.e. 70% of voids and 30% of amorphous Ge) and/or germanium oxide. The formation of a thin GeO_2 layer on the surface of Ge films deposited by evaporation or sputtering has been reported by other authors [21,46,52].

The results indicate that the substrate temperature during deposition has a significant effect on the optical and structural properties of germanium films. An increase of T_s from room temperature up to 300 °C, results in a clear increase of the optical gap energy (from 0.71 up to 0.90 eV) and the $B^{1/2}$ parameter (from 445 up to 609 $\text{eV}^{-1/2} \text{cm}^{-1/2}$), that should be related to an improvement of the structural order in the film [14,16]. As the temperature increases up to 200 °C, it is observed that a higher refractive index and a lower extinction coefficient in the mid-infrared range, suggest that the film structure becomes denser and with fewer defects. The

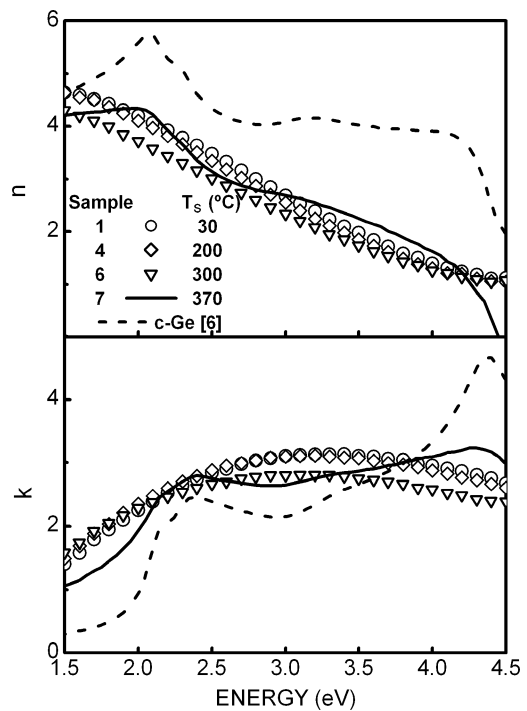


Fig. 4. Optical constants of Ge thin films deposited on sapphire substrates at different temperatures (cf. Table 1), estimated by ellipsometry.

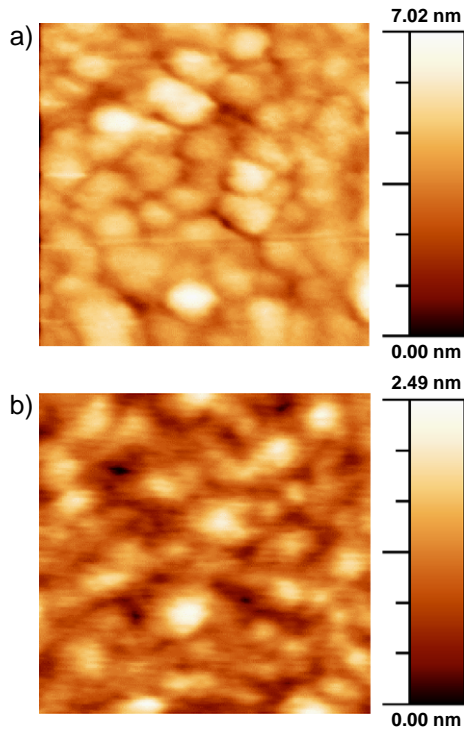


Fig. 5. AFM topographic images ($1 \times 1 \mu\text{m}^2$) of the surfaces of SiO thin films deposited on sapphire substrates at 200°C and with different deposition rates. a) 0.3 nm/s , sample 3; b) 3.0 nm/s , sample 5 (cf. Table 2).

increase in the mean grain size obtained by AFM in this temperature range is consistent with these results. A further increase of T_s up to 300°C reduces the refractive index, due to the thickening of the low-index surface layer and probably to the formation of grooves observed by AFM.

The films grown at 370°C are polycrystalline, in good agreement with the results of other authors, that report crystallisation temperatures in germanium thin films between 250 and 400°C [14–16,22,23,25]. The presence of a crystalline phase explains the decrease of the refractive index, reaching values close to that expected of crystalline germanium. Nevertheless, the observed decrease of the optical gap and the $B^{1/2}$ parameter when T_s increases up to 370°C , indicates a significant structural disorder, which must be related to the presence of both crystalline and amorphous phases, as indicated by ellipsometry. Finally, the high value of the extinction coefficient in the mid-infrared range obtained for sample 7 might be due to scattering losses [53], related to the high surface roughness deduced from the AFM images.

3.2. SiO thin films

Silicon monoxide thin films grown on sapphire substrates at different temperatures and with different deposition rates have been analysed. Table 2 summarises the deposition parameters of the samples and includes the values for the refractive index at $4 \mu\text{m}$ ($n_{4 \mu\text{m}}$) and for the

layer physical thickness (d_{exp}), as determined from their optical characterisation.

Representative AFM images of samples 3 and 5 are shown in Fig. 5. This figure shows that increasing the deposition rate from 0.3 up to 3.0 nm/s results in a clear decrease of the rms roughness from 0.9 nm for sample 3 (Fig. 5a) down to 0.4 nm for sample 5 (Fig. 5b). The calculated mean grain size diminishes slightly, from 107 down to 90 nm .

Fig. 6 shows the refractive index and extinction coefficient of representative samples, as derived from the analysis of the transmission spectra in the wavelength range from 1.25 to $5 \mu\text{m}$. Fig. 6 indicates a significant effect of deposition rate, with a higher refractive index for higher rates, and a weaker influence of substrate temperature. All the samples are transparent in the mid-infrared range but sample 3, grown with the lowest deposition rate (i.e. 0.3 nm/s), shows a higher extinction coefficient.

Fig. 7 shows the experimental transmission spectrum of sample 7 and that corresponding to the sapphire substrate. The spectrum calculated using the optical constants and thickness obtained for this sample by reverse synthesis is also included. An absorption band is clearly observed in the experimental curve at around $3 \mu\text{m}$, which is usually assigned to OH groups from water adsorbed in structural voids [54–56]. Apart from this absorption region, the agreement between experimental and calculated curves is excellent.

In the case of porous films with low refractive index and low absorption, Laux et al. [54] have proposed a method to estimate the packing density from the analysis of the OH-related absorption band. Considering that all the voids in the

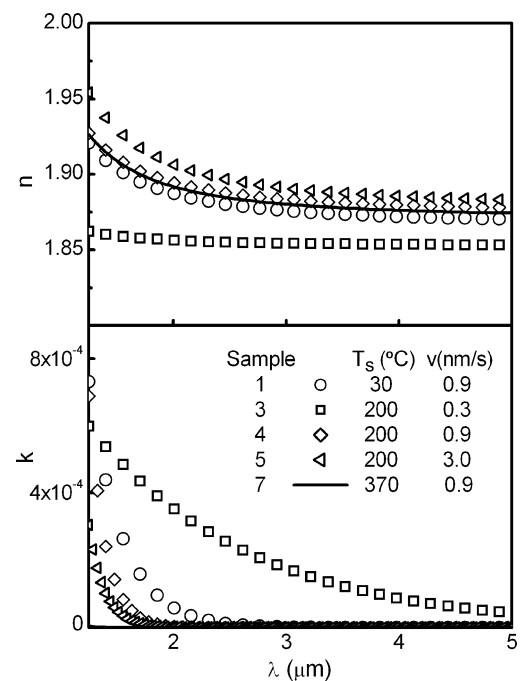


Fig. 6. Optical constants of SiO thin films grown on sapphire substrates with different deposition conditions (cf. Table 2), estimated by reverse synthesis of transmission spectra.

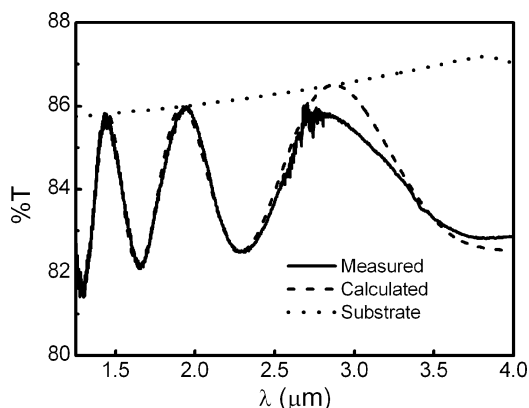


Fig. 7. Measured transmission spectra of a representative SiO sample (sample 7 in Table 2) and the corresponding sapphire substrate. Also included is the transmittance calculated using the optical constants and thickness estimated for sample 7 by reverse synthesis.

film are filled with water, the packing density, p , may be estimated by:

$$p = 1 - \frac{N_H}{N_H^*} \approx 1 - \gamma \frac{A}{d(n^2 + 2)^2} \quad (4)$$

where N_H^* and N_H are the hydrogen atom density in water and in the film studied respectively. γ is a parameter involving water refractive index at 2.9 μm , the dielectric constant of vacuum, the speed of light, the hydrogen atomic mass and the so-called Szigeti charge (z_H). This Szigeti charge is related to the distortion of the electric charge distribution associated with the chemical bond and depends on the layer material [54]. The second term of Eq. (4) also includes the thickness (d) and refractive index at a wavelength of 2.9 μm (n) of the film. Finally, A is the OH-related absorption band area as obtained from the ratio between the experimental transmission spectrum and the simulated one (cf. Fig. 7).

The parameter Γ , defined as:

$$\Gamma \equiv \frac{A}{d(n^2 + 2)^2} \quad (5)$$

has been calculated from the respective transmission spectra of the samples listed in Table 2 and the corresponding

thickness and refractive index at 2.9 μm . The minimum value of this parameter (i.e. Γ_{\min}), which corresponds to the densest film, has been obtained for sample 5 grown at 200 $^\circ\text{C}$ with the highest deposition rate (3.0 nm/s). Fig. 8 shows the variation of Γ_{\min}/Γ for different substrate temperatures (a) and deposition rates (b) of the films in Table 2. This ratio, and subsequently the layer density, is observed to increase slightly as T_s increases and more significantly as the deposition rate increases. The presence of a higher amount of voids in the SiO film grown at 0.3 nm/s is in agreement with its higher surface roughness (cf. Fig. 5) and would account for its higher extinction coefficient, as observed in Fig. 6 [53].

A detailed characterisation of similar SiO films has been published recently [57]. The analysis of the IR absorption band related to the oxygen stretching mode of Si–O–Si bond indicates that the structure of these SiO films is formed by tetrahedral units $\text{Si–O}_y\text{–Si}_{4-y}$ ($y=1-4$), according to the random bonding model (RBM) [39,40]. Nevertheless, a deviation from the pure RBM structure is found both in the relative concentration of the different tetrahedra and in the presence of an additional contribution of Si–O₄ tetrahedra. No significant variation is observed in the concentration of the oxygen-containing tetrahedra as the deposition rate varies from 0.3 to 3 nm/s, for films grown on substrates at 200 $^\circ\text{C}$. On the other hand, a slight increase of the oxygen content in the films is confirmed as the substrate temperature is raised from room temperature up to 370 $^\circ\text{C}$.

According to the results presented above, an increase in the substrate temperature during deposition leads to a slight increase of the SiO layer density (cf. Fig. 8), and consequently of the refractive index, as well as to a slight increase of the oxygen content [57] that tends to decrease the refractive index. The net effect is an almost constant value of the refractive index ($n_{4\ \mu\text{m}}=1.87-1.88$) for substrate temperature increasing from 30 up to 370 $^\circ\text{C}$. On the other hand, the observed increase in refractive index with deposition rate must be related to the formation of a denser film, as suggested by the analysis of packing density (cf. Fig. 8). Further measurements should be performed to

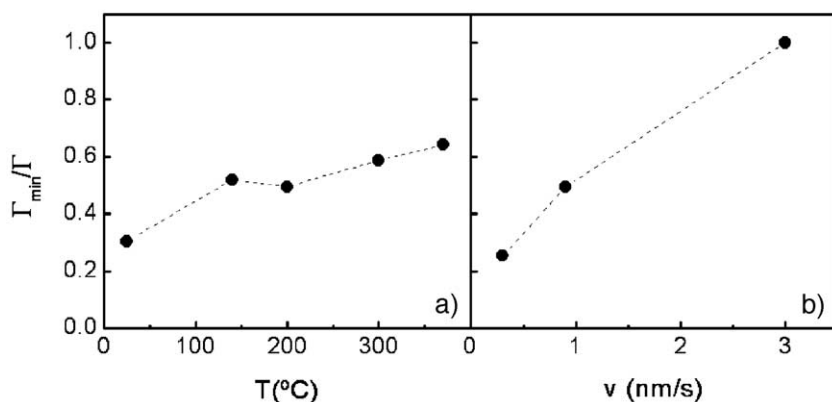


Fig. 8. Packing density of SiO thin films as a function of substrate temperature (a) and deposition rate (b), represented by the normalised value of parameter Γ as defined by equation Eq. (5) in the text.

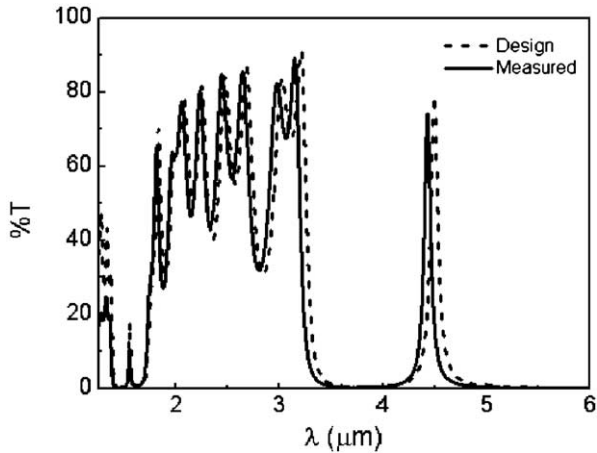


Fig. 9. Transmission spectra corresponding to the ten-layer filter design and measured for a representative experimental multilayer.

define any variation of film stoichiometry with the deposition rate. In any case, as the oxygen-containing tetrahedra concentration must be fairly constant for deposition rates between 0.3 and 3 nm/s [57], only variations in Si_4 tetrahedra concentration may occur.

3.3. Multilayer systems

Taking into account that thin films in multilayer interference coatings must be dense and have low absorption in the wavelength range defined for the intended application, the appropriate deposition conditions for silicon monoxide and germanium in multilayer systems for the mid-infrared range of the spectrum may be selected.

According to the previous analysis of single Ge and SiO layers, a substrate temperature of 200 °C would be adequate for the preparation of multilayer systems. A lower temperature results in less dense silicon monoxide films and a higher value of T_s gives rise to a rougher surface in germanium films. A deposition rate of 0.9 nm/s may be selected for Ge films, to avoid problems with source stability at higher rates in long processes, while a value of 3 nm/s is the best choice for SiO films in order to obtain denser films.

A ten-layer bandpass filter for the mid-infrared range has been designed and prepared using the parameter setting, as already described for SiO and Ge single layers. The coating design corresponds to a Fabry–Perot cavity

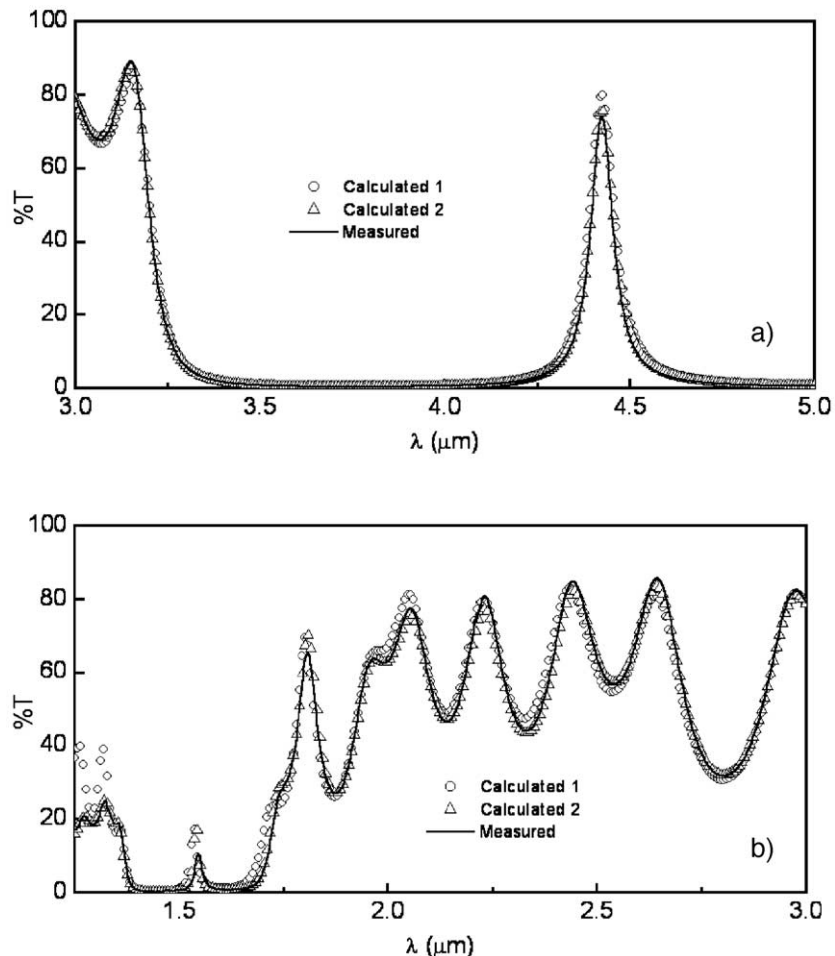


Fig. 10. Transmission spectrum measured for a representative ten-layer filter and calculated with the results of reverse synthesis varying only layer thicknesses (calculated 1) and varying layer thickness and optical constants of SiO and Ge (calculated 2).

with a high refractive-index spacer, centered at a wavelength of 4.49 μm . The measured transmittance curve of a representative filter in the wavelength range from 1.25 to 6 μm is compared with that corresponding to the design in Fig. 9. The measured spectrum is consistent with the design, but a significant shift to lower wavelengths is observed.

In order to obtain the experimental thickness of the ten layers, the filter has been analysed, using the reverse synthesis of the transmission spectrum. In the reverse synthesis procedure, the dispersion functions are set constant and equal for all layers of each material within the coating. The mean optical constants obtained from three samples grown under the same conditions as in the multilayer, but with a nominal thickness of around 1800 nm, have been considered for each material.

The result of the filter characterisation indicates that the experimental thicknesses are lower than those corresponding to the design for both SiO and Ge. The mean deviation of the thickness for SiO layers is 2%, while that for Ge layers is 1%. The transmission spectrum calculated using the results of this characterisation, labelled as “Calculated 1”, is compared with the measured curve in Fig. 10. A fairly good agreement between the two curves is observed. Indeed, although some slight discrepancies between the calculated and experimental spectra are observed in the near-infrared range (Fig. 10b), the calculated spectrum consistently reproduces the filter response in the mid-infrared range (Fig. 10a).

A second reverse synthesis analysis of the filter spectrum has been carried out, allowing for optical constant variations. The parameters of dispersion functions for n and k of both SiO and Ge, as well as the thickness of the ten layers, were varied to obtain the best fit to the experimental transmittance. The results of the previous characterisation were used as starting point, in order to reduce the inherent inaccuracy of the optimisation procedure when many variables are considered [44,47,58].

As in the first analysis, the resulting thicknesses are lower than those corresponding to the design, but in this case the mean deviation of the thickness is 1% for both SiO and Ge layers. Fig. 11 shows the refractive index and extinction coefficient estimated for SiO and Ge films in the ten-layer filter, as compared to the initial values. It must be noted that the mean extinction coefficient of single SiO layers is negligible in the scale considered in this figure. The optical constants depicted in Fig. 11 indicate that Ge thin films have similar optical constants in multilayer and single layer configurations. On the contrary, SiO thin films show slightly lower refractive index, as well as higher extinction coefficient in the low wavelength range, in the multilayer system as compared with single layers. These slight variations of the silicon monoxide layer properties account for the better agreement between the spectrum labelled as “Calculated 2” in Fig. 10 and the experimental one, especially in the near-infrared range.

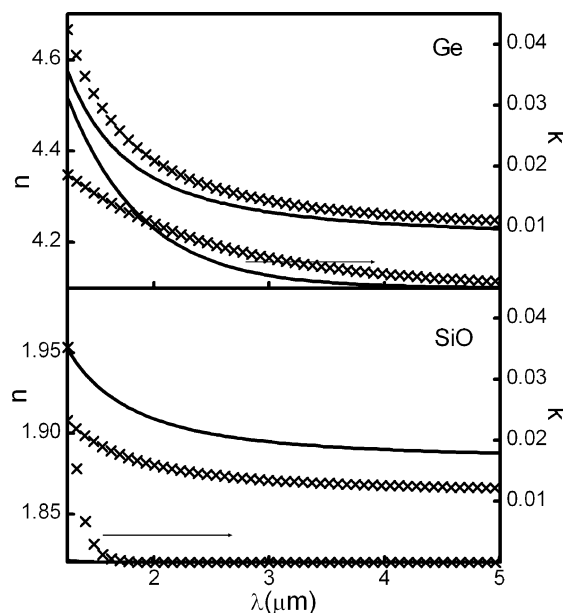


Fig. 11. Optical constants of Ge and SiO as estimated by reverse synthesis from the transmission spectrum of the ten-layer filter depicted in Fig. 9 (crosses), compared to the design values (solid curves).

The optical characterisation of the representative ten-layer filter indicates that the departure of experimental transmittance from design is mainly due to thickness deviations, which must be related to inadequate quartz-crystal monitor calibration. Only for fine adjustment of the filter response in the near-infrared range, some deviations of the silicon monoxide optical constants in the multilayer system must be considered.

To account for the different properties of SiO thin films in single and multilayer configurations, several effects should be considered, such as contamination between different materials [42], interface layer formation [41,59], variations in porosity [42] or interface roughness [60]. An effect of layer thickness on the optical constants may exist as well [41].

4. Conclusions

Structural, morphological and optical properties of Ge and SiO thin films prepared in different evaporation conditions are studied using XRD, AFM, ellipsometry and spectrophotometry.

The results of Ge thin films characterisation indicate that the substrate temperature during deposition has a significant effect on their optical and structural properties. An increase of T_s from room temperature up to 200 $^{\circ}\text{C}$, gives rise to a higher refractive index and a lower extinction coefficient in the mid-infrared range, mainly caused by the formation of denser films with less defects. A further increase of T_s up to 300 $^{\circ}\text{C}$ results in a reduction of the refractive index, due to an increase of the surface layer thickness. Finally, for T_s equal to 370 $^{\circ}\text{C}$ the film is, in fact, a mixture of crystalline

and amorphous phases, with a high structural disorder and surface roughness. Related to these structural properties, the refractive index approaches the value of crystalline germanium and the extinction coefficient in the mid-infrared range increases significantly.

The study of silicon monoxide single layers indicates a porous structure in all the evaporation conditions considered. According to the results, an increase in the substrate temperature during film deposition gives rise to a slight increase of both the layer density and the oxygen content [57], so that the refractive index in the mid-infrared remains almost constant for substrate temperature between 30 and 370 °C. On the other hand, an increase in refractive index with deposition rate is observed, related to the formation of denser films.

Taking into account the results of the single layers analysis, deposition conditions adequate for both SiO and Ge thin films in multilayer systems for the mid-infrared range of the spectrum are selected. A ten-layer bandpass filter, centered at a wavelength of 4.49 μm with a single cavity Fabry–Perot configuration was designed considering experimental optical constants for both materials. The optical characterisation of a representative filter, prepared with the selected deposition conditions, indicates that the departure of experimental transmittance in the mid-infrared range from the design is mainly due to thickness deviations.

Acknowledgements

Thanks are due to the Servicio Interdepartamental de Investigación of the Universidad Autónoma de Madrid for the XRD patterns and to all the members of the Optical Coatings group of CIDA for their help in the experimental work.

References

- [1] A. Macleod, *Thin Film Optical Filters*, 3rd ed., Institute of Physics Publishing, Bristol, 2001.
- [2] J.D. Rancourt, *Optical Thin Films. User Handbook*, SPIE Optical Engineering Press, Washington, 1996.
- [3] F. López, J. de Frutos, *Sens. Actuators, A, Phys.* 37–38 (1993) 502.
- [4] G.J. Hawkins, R. Hunneman, *Proc. SPIE* 2210 (1994) 639.
- [5] F. Lemarquis, G. Marchand, C. Amra, C. Buil, B. Cousin, G. Otrio, *Appl. Opt.* 38 (1999) 4182.
- [6] E.D. Palik, *Handbook of Optical Constants of Solids*, Academic Press, Orlando, 1985.
- [7] J.A. Savage, *Infrared Optical Materials and their Antireflection Coatings*, Adam Hilger Ltd, Bristol, 1985.
- [8] J. Wales, G.J. Lovitt, R.A. Hill, *Thin Solid Films* 1 (1967) 137.
- [9] H. Rafla-Yuan, J.D. Rancourt, M.J. Cumbo, *Appl. Opt.* 36 (1997) 6360.
- [10] A. Ghosh, P. Kant, P.K. Bandyopadhyay, P. Chandra, O.P. Nijhawan, *Infrared Phys. Technol.* 40 (1999) 49.
- [11] G.J. Hawkins, R. Hunneman, R. Sherwood, B.M. Barrett, *Appl. Opt.* 39 (2000) 5221.
- [12] K.L. Chopra, S.K. Bahl, *Phys. Rev. B* 1 (1970) 2545.
- [13] A.H. Clark, *J. Non-Cryst Solids* 2 (1970) 52.
- [14] M.L. Theye, *Opt. Commun.* 2 (1970) 329.
- [15] G. Jungk, *Phys. Status Solidi, B Basic Res.* 44 (1971) 239.
- [16] G.A.N. Connell, R.J. Temkin, W. Paul, *Adv. Phys.* 22 (1973) 643.
- [17] J. Tauc, *Amorphous and Liquid Semiconductors*, Plenum, New York, 1974.
- [18] R. Zallen, *The Physics of Amorphous Solids* (Wiley Classics Library). John Wiley and Sons Inc., New York, 1998.
- [19] E.H. Hirsch, I.K. Varga, *Thin Solid Films* 69 (1980) 99.
- [20] J.E. Yehoda, B. Yang, K. Vedam, R. Messier, *J. Vac. Sci. Technol., A, Vac. Surf. Films* 6 (1988) 1631.
- [21] J.C.G. de Sande, C.N. Afonso, J.L. Escudero, R. Serna, F. Catalina, E. Bernabéu, *Appl. Opt.* 31 (1992) 6133.
- [22] N. Inoue, Y. Yasuoka, *Jpn. J. Appl. Phys.* 27 (1988) 1437.
- [23] H. Kobayashi, N. Inoue, T. Uchida, Y. Yasuoka, *Thin Solid Films* 300 (1997) 138.
- [24] F. Scarinci, M. Fiordelisi, R. Calarco, S. Lagomarsino, L. Colace, G. Masini, G. Barucca, S. Coffa, S. Spinella, *J. Vac. Sci. Technol. B* 16 (1998) 1754.
- [25] I. Günal, A.F. Qasrawi, *J. Mater. Sci.* 34 (1999) 5033.
- [26] M. Mulato, D. Toet, G. Aichmayr, A. Spangenberg, P.V. Santos, I. Chambouleyron, *J. Non-Cryst. Solids* 227–230 (1998) 930.
- [27] N. Motta, A. Sgarlata, R. Calarco, J. Castro Cal, Q. Nguyen, P. Proposito, A. Balzarotti, M. de Crescenzi, *J. Vac. Sci. Technol. B* 16 (1998) 1555.
- [28] D.V. Melnikov, J.R. Chelikowsky, *Solid State Commun.* 127 (2003) 361.
- [29] G. Hass, C.D. Salzberg, *J. Opt. Soc. Am.* 44 (1954) 181.
- [30] A. Lehmann, L. Schumann, K. Hübner, *Phys. Status Solidi, B Basic Res.* 121 (1984) 505.
- [31] M. Nakamura, Y. Mochizuki, K. Usami, Y. Itoh, T. Nozaki, *Solid State Commun.* 50 (1984) 1079.
- [32] P.G. Pai, S.S. Chao, Y. Takagi, G. Lucovsky, *J. Vac. Sci. Technol., A, Vac. Surf. Films* 4 (1986) 689.
- [33] K. Haga, H. Watanabe, *Jpn. J. Appl. Phys.* 29 (1990) 636.
- [34] P. González, D. Fernández, J. Pou, E. García, J. Serra, B. León, M. Pérez-Amor, T. Szörényi, *Appl. Phys. A* 57 (1993) 181.
- [35] L. He, T. Inokuma, Y. Kurata, S. Hasegawa, *J. Non-Cryst. Solids* 185 (1995) 249.
- [36] P.V. Bulkin, P.L. Swart, B.M. Lacquet, *J. Non-Cryst. Solids* 226 (1998) 58.
- [37] H. Rinnert, M. Vergnat, G. Marchal, *Mater. Sci. Eng., B, Solid-State Mater. Adv. Technol.* 69–70 (2000) 484.
- [38] R.J. Temkin, *J. Non-Cryst. Solids* 17 (1975) 215.
- [39] H.R. Philipp, *J. Phys. Chem. Solids* 32 (1971) 1935.
- [40] H.R. Philipp, *J. Non-Cryst. Solids* 8–10 (1972) 627.
- [41] B.T. Sullivan, K. Birt, *Appl. Opt.* 34 (1995) 5684.
- [42] S.A. Kumar, C.L. Nagendra, H.G. Shanbhogue, G.K.M. Thutupalli, *Opt. Eng.* 38 (1999) 368.
- [43] R.Y. Tsai, C.S. Chang, C.W. Chu, T. Chen, F. Dai, D. Lin, S. Yan, A. Chang, *Appl. Opt.* 40 (2001) 1593.
- [44] M. Ylilammi, T. Ranta-aho, *Thin Solid Films* 232 (1993) 56.
- [45] J. Ciosek, J.A. Dobrowolski, G.A. Clarke, G. Laframboise, *Appl. Opt.* 38 (1999) 1244.
- [46] A.A. Al-Mahasneh, H.A. Al Attar, I.S. Shahin, *Opt. Commun.* 220 (2003) 129.
- [47] A.V. Tikhonravov, M.K. Trubetskov, *Proc. SPIE* 5250 (2004) 406.
- [48] P. Meredith, G.S. Buller, A.C. Walker, *Appl. Opt.* 32 (1993) 5619.
- [49] W.G. Driscoll, W. Vaughan, *Handbook of Optics*, McGraw-Hill Inc., 1978.
- [50] S.H. Wemple, M. DiDomenico Jr., *Phys. Rev. B* 3 (1971) 1338.
- [51] R.M. Bueno, J.F. Trigo, J.M. Martínez-Duart, E. Elizalde, J.M. Sanz, *J. Vac. Sci. Technol., A, Vac. Surf. Films* 13 (1995) 2378.
- [52] P.J. McMarr, J.R. Blanco, *Appl. Opt.* 27 (1988) 4265.
- [53] C.K. Carniglia, D.G. Jensen, *Appl. Opt.* 41 (2002) 3167.
- [54] S. Laux, W. Richter, *Appl. Opt.* 35 (1996) 97.

- [55] A. Brunet-Bruneau, D. Souche, S. Fisson, V.N. Van, G. Vuye, F. Abeles, J. Rivory, *J. Vac. Sci. Technol., A, Vac. Surf. Films* 16 (1998) 2281.
- [56] N. Benissad, K. Aumaille, A. Granier, A. Goulet, *Thin Solid Films* 384 (2001) 230.
- [57] G. Pérez, J.M. Sanz, *Thin Solid Films* 416 (2002) 24.
- [58] J. Sancho-Parramón, J. Ferré-Borrull, S. Bosch, M.C. Ferrara, *Appl. Opt.* 42 (2003) 1325.
- [59] N. Brun, C. Colliex, J. Rivory, K. Yu-Zhang, *Microsc. Microanal. Microstruct.* 7 (1996) 1.
- [60] C.L. Mitsas, D.I. Siapkas, *Appl. Opt.* 34 (1995) 1678.